ЖУРНАЛ СТРУКТУРНОЙ ХИМИИ

2016. Том 57, № 1 *Январь – февраль* *С. 198 – 202*

UDC 541.65:535.42

ZnO AND MgO NANOPARTICLES: SYNTHESIS AND COMPARATIVE STUDY ON THEIR PROPERTIES

A. Bagheri ghomi

Department of Chemistry, Center Tehran Branch, Islamic Azad University, Tehran, Iran
E-mail: azbagheri@gmail.com

Received January, 8, 2015

We report the optical and structural properties of ZnO and MgO nanoparticles. The samples are obtained by a simple method using a new template of hexamethylene tetramine. The optical properties of the samples are studied by UV-visible spectroscopy. Their crystal structure and morphology are studied by XRD and scanning electron microscopy. The absorption spectra of MgO and ZnO show that the optical band gaps are 4.27 eV and 3.02 eV, respectively. In this investigation the photocatalytic degradation of indigo carmine (IC) in water is studied. The effects of some parameters such as pH, amount of catalyst, initial concentration of dye, are examined.

DOI: 10.15372/JSC20160124

K e y w o r d s: nanoparticle, ZnO, MgO, photocatalyst, band gap.

Metal oxide nanomaterials exhibit unique physical and chemical properties and have potential applications in magnetism, catalysis, electro-optical devices, sensors, and nanodevices [1—3]. Among semiconducting catalysts, zinc oxide (ZnO) has been extensively studied due to its low cost, nontoxicity, outstanding stability, and high efficiency [4—7]. Owing to their large surface area, nanosized ZnO particles can be effectively utilized to enhance photocatalytic activity [8—11]. Every solid has its own characteristic energy band structure. A variation in the band structure is responsible for the wide range of electrical characteristics observed in various materials. In semiconductors and insulators, electrons are confined to a number of energy bands and forbidden from other regions. The conductivity of intrinsic semiconductors is strongly dependent on the band gap.

Magnesium oxide (MgO) as a versatile oxide material with assorted properties such as a large band gap, excellent thermodynamic stability, low dielectric constant, and low refractive index, finds extensive applications in catalysis, ceramics, toxic waste remediation, antibacterial materials, and as an additive in refractory, paint and superconductor products [12—16].

Among various methods of the chemical synthesis there are the sol-gel method [17], hydrothermal [18], chemical vapor deposition [19], pulsed laser deposition [20], and molecular beam epitaxy [21]. These preparation methods involve complex procedures, sophisticated apparatus/equipment, rigorous experimental conditions, high-temperature annealing. Hence, in this work, we have synthesized ZnO and MgO nanostructures by a simple reflux method. The photocatalytic performance of the synthesized MgO nanoparticles was evaluated by monitoring the photodegradation of indigo carmine (IC) dye under UV light irradiation.

EXPERIMENTAL

Apparatus. For the UV/photocatalyst process, irradiation was performed in a two-liter batch photoreactor with four mercury lamps (Philips 8W (UV-C)). A magnetic stirrer was used to ensure complete mixing in the tank (stirring speed = 250 rpm) and air was dispersed at a flow rate of 1 l/min using an air diffuser to supply oxygen for the enhancement of photo-oxidation. A Shimadzu 2101 UV-Vis spectrophotometer was employed for absorbance measurements using silica cells with a 1-cm path length. The morphology of nanostructured ZnO was determined by scanning electron microscopy (SEM) on a Holland Philips XL30 microscope. X-ray diffraction (XRD) analysis was carried out at room temperature using a Holland Philips Xpert X-ray powder diffractometer with CuK_α radiation (λ = 0.15406 nm), over the 2θ collection range 0—80°.

Preparation of ZnO. 4 mmol NaOH was dissolved in 75 ml distilled water under stirring. Then the hexamethylene tetramine template (4 mmol) was added to the solution. Zinc acetate (1 mmol) was added to the mixture. The mixture was refluxed for 4 h at 80 °C. After cooling to room temperature, the precipitate was collected by filtration and several times washed with distilled water and ethanol. ZnO was obtained by centrifugation and drying of the precipitate at room temperature.

Preparation of MgO. Magnesium hydroxide $Mg(OH)_2$ is considered as the precursor of MgO nanoparticles. $Mg(OH)_2$ was prepared by stirring a mixture of aqueous solutions of magnesium acetate, hexamethylene tetramine template, and sodium hydroxide at room temperature for 3 h. The $Mg(OH)_2$ precipitate was filtered and dried at 80 °C for 1 h. Then it was calcinated at 500 °C for 3 h in a muffle furnace.

Procedure. For the degradation of IC, a solution containing a known concentration of the dye and the catalyst was prepared and was allowed to equilibrate for 30 min in the darkness. The decolorization experiments were carried out in 500 ml of 15 ppm IC. The IC concentration was determined by measuring the absorption intensity at its maximum absorbance wavelength at 610 nm with a UV-Vis spectrophotometer. Decolorization efficiency was deduced from Eq. (1)

$$\% \text{ Decolorization } X = \frac{C_0 - C}{C_0}, \quad (1)$$

where Co is the initial IC concentration, C is the IC concentration at a certain reaction time.

RESULTS AND DISCUSSION

Characterization of nanoparticles. The surface morphologies of the products were studied by SEM as shown in Fig. 1. The ZnO and MgO morphologies were nanosheets and nanospheres, respectively.

Fig. 2, *a* shows XRD patterns of the obtained nanostructures. All the diffraction peaks can be well indexed to the cubic MgO phase reported in JCPDS (card No. 78-0430).

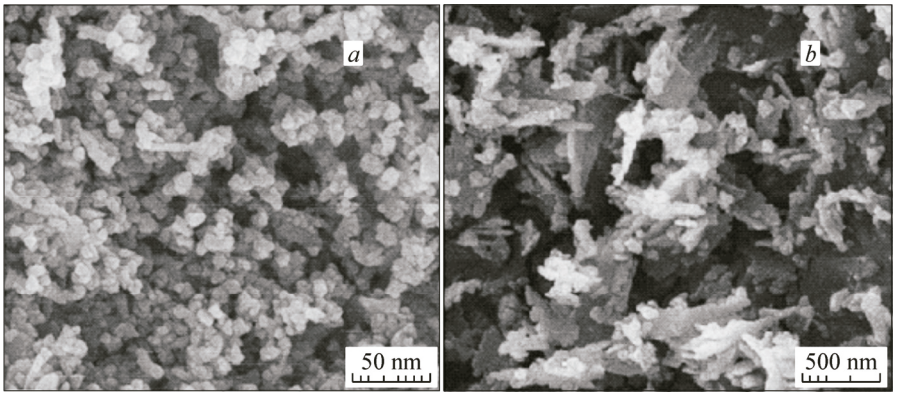

Fig. 1. SEM image MgO (*a*) ZnO (*b*)

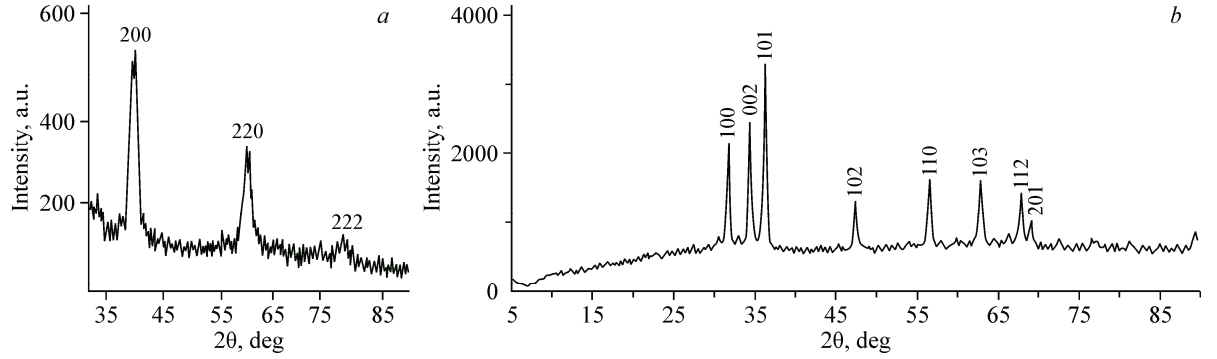

Fig. 2. X-ray diffraction pattern of MgO (*a*) ZnO (*b*)

Powder XRD patterns of ZnO nanoparticles are depicted in Fig. 2. Pattern 2a was obtained from the ZnO nanoparticles prepared according to the method described elsewhere. All the prominent peaks in the pattern corresponded to the wurtzite structure of ZnO, which can be indexed based on JCPDS file No. 36-1451. No other characteristic peaks of the impurities are observed, indicating the high purity of the final products.

These results indicate the high purity of ZnO and MgO nanoparticles. The obtained particles were found to exhibit similar characteristic XRD peaks. Average crystallite sizes of the products were calculated using Scherrer′s formula: $D = 0.9\lambda/\beta\cos\theta$ [22], where D is the diameter of the nanoparticles, $\lambda(\mathrm{Cu}K_\alpha) = 1.5406$ Å, and β is the full-width at half-maximum of the diffraction lines. The calculated average particles of MgO and ZnO are 7 nm and 28 nm, respectively.

Optical properties. The absorption edges for MgO and ZnO appeared at 290 nm and 411 nm, respectively (Fig. 3). The band gap energy can be estimated based on the corresponding absorption edges according to Eq. (2) [23]:

$$E_g = 1240\lambda^{-1}, \quad (2)$$

where E_g is the band gap energy (eV) and λ is the wavelength (nm). The band gap energies are 4.27 eV and 3.02 eV, respectively.

Photocatalytic results. The effects of different parameters in IC adsorption on the properties of resulted MgO and ZnO, such as pH, were also examined. The results indicated that nanoparticles showed an adsorption capacity. When the solutions are left in darkness for 15 min, the IC concentrations in all solutions decreases remarkably. This is due to the adsorption of dye molecules on the surface of these photocatalysts.

The photodegradation conversion of IC decreases with an increase in the initial IC concentration. The presumed reason is that when the initial dye concentration is increased, more and more dye molecules are adsorbed on the photocatalyst surface. The degradation of IC at different pH from 3 to 10 were studied, and the best results were obtained in the acidic solution (pH = 3).

The highest and lowest adsorptions is attributed to MgO and ZnO photocatalysts. It can decolorize 60 % IC solution in 120 min and after 180 min the color can be removed.

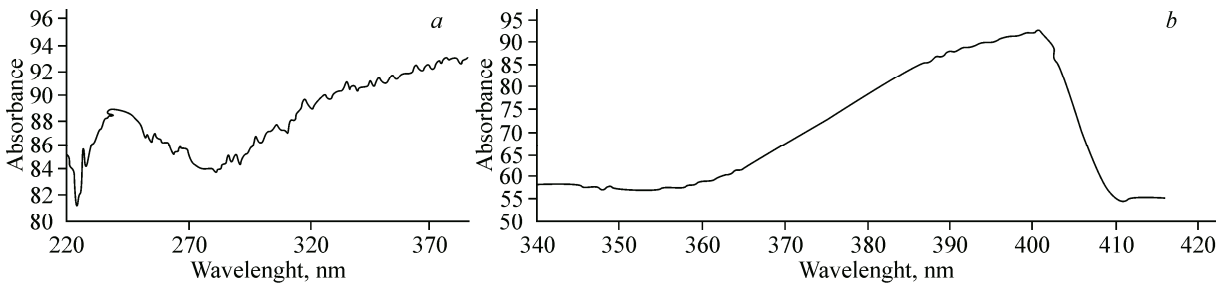

Fig. 3. Solid-state UV-Vis spectrum of MgO (*a*) ZnO (*b*)

Table 1

Physicochemical characteristics of nanoparticles

Sample	Morphology	Absorption edge, nm	Band gap energy, eV	Crystallite size, nm
MgO	Nanosheet	290	4.27	7
ZnO	Nanosphere	411	3.02	28

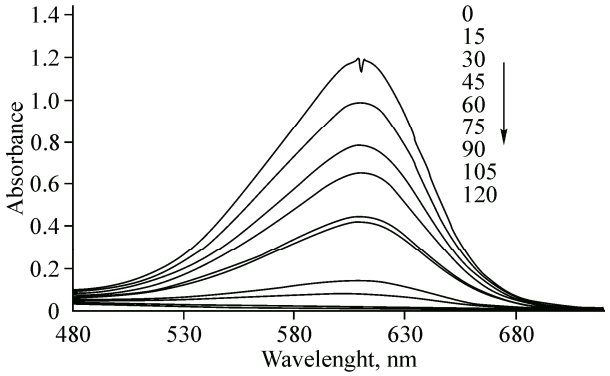

Fig. 4. UV-Vis spectra of IC in aqueous catalyst (MgO) dispersion irradiated with a mercury lamp light at pH = 3, T = 298 K, at: t = 0, 15, 30, 45, 60, 75, 90, 105, 120 min

The absorbance of IC solutions during the catalytic process with MgO at the initial and after 2 h irradiation time versus λ is shown in Fig. 4. The decrease in absorption peaks of IC at λ_{max} = 610 nm in this figure indicates a rapid degradation of the dye.

In this research, the MgO photocatalyst with the nanosheet morphology shows higher photocatalytic efficiency. The crystallite size and band gap of MgO are the smallest and largest, respectively (Table 1).

The research shows that the morphology and particle size play the important role in the adsorption of dye molecules. The smaller the crystallite size, the larger the band gap and the higher the photodecolorization are.

CONCLUSIONS

This band gap is very close to that of GaN, and GaN has been the subject of much research over the past years, even being incorporated into the recent Blu-ray Drives. However, ZnO has some significant advantages in its high free exciton binding energy (60 meV compared to 21—25 meV for GaN) that is responsible for the efficient exciton emission at room temperature. Band-gap engineering of ZnO can be achieved by alloying with MgO.

The results obtained proved that nano MgO and ZnO were successfully prepared via the reflux and using the template. The XRD data show the optimum temperature for the decomposition of $Mg(OH)_2$ to form nano MgO. The calculation from the XRD data proved the formation of nano MgO with a particle size *ca* 7 nm. An explanation for the formation of ZnO can involve the role of preformed nuclei and the template used to control the growth rate of various facets of the preformed nuclei. In the initial stage of the reflux, complex $Zn(OH)_4^{2-}$ is formed. The growth unit for the ZnO crystal is considered to be $Zn(OH)_4^{2-}$ [23—26]. MgO and ZnO can be used in the form of fine powders or crystals dispersed in wastewater treatment applications. The degradation conversion of IC decreases with an increase in the initial IC concentration. pH is one of the main factors and the optimum pH was obtained to be about 3.

We wish to thank the Islamic Azad University Center Tehran Branch for its invaluable support through the project.

REFERENCES

1. *Comini E., Baratto C., Faglia G., Ferroni M., Vomiero A., Sberveglieri G.* // Prog. Mater. Sci. – 2009. – **549**. – P. 1 – 67.
2. *Kim M.H., Lee B., Lee S., Larson C., Baik J.M., Yavuz C.T., Seifert S., Vajda S.* // Nano Lett. – 2009. – **9**. – P. 4138 – 4146.
3. *Shen G.Z., Chen P.C., Ryu K., Zhou C.W.* // J. Mater. Chem. – 2009. – **19**. – P. 828 – 839.
4. *Akyol A., Bayramoglu M.* // J. Hazard. Mater. – 2010. – **175**. – P. 484 – 491.
5. *Khan S.B., Faisal M., Rahman M.M., Jamal A.* // Talanta. – 2011. – **85**. – P. 943 – 949.
6. *Li J., Lu G., Wang Y., Guo Y., Guo Y.* // J. Colloid Interface Sci. – 2012. – **377**. – P. 191 – 196.
7. *Wang H., Xie C., Zhang W., Cai S., Yang Z., Gui Y.* // J. Hazard. Mater. – 2007. – **141**. – P. 645 – 652.

8. *Xiang Q., Meng G., Zhang Y., Xu J., Xu P., Pan Q., Yu W.* // Sens. Actuator B-Chem. – 2010. – **143**. – P. 635 – 640.
9. *Xia J., Wang A., Liu X., Su Z.* // Appl. Surf. Sci. – 2011. – **257**. – P. 9724 – 9732.
10. *Ba-Abbad M.M., Kadhum A.A.H., Mohamad A.B., Takriff M.S., Sopian K.* // J. Alloy. Compd. – 2013. – **550**. – P. 63 – 70.
11. *Silva R.F.* Filmes de óxido de zinco dopado com alumínio ou európio: Preparação ecaracterização. Tese (Doutorado), Faculdade de Filosofia, Ciências e Letras de Ribeirão Preto, 2001.
12. *Abrarov S.M., Yuldashev Sh.U., Lee S.B., Kang T.W.* // J. Luminescence. – 2004. – **109**. – P. 25 – 29.
13. *Sousa V.C. et al*. // Internat. J. Inorg. Mater. – 1999. – **1**. – P. 235 – 241.
14. *Wang J., Gao L.* // Solid State Commun. – 2004. – **132**. – P. 269 – 271.
15. *Duan G., Yang X., Chen J., Huang G., Lu L., Wang X.* // Powder Technol. – 2007. – **172**. – P. 27 – 29.
16. *Niu H., Yang Q., Tang K., Xie Y.* // Scr. Mater. – 2006. – **54**. – P. 1791 – 1796.
17. *Shah M.A., Qurashi A.* // J. Alloys Compd. – 2009. – **482**. – P. 548 – 551.
18. *Wang W., Qiao X., Chen J., Tan F., Li H.* // Mater. Charact. – 2009. – **60**. – P. 858 – 862.
19. *Qiu T., Wu X.L., Jin F.Y., Huang A.P., Chu P.K.* // Appl. Surf. Sci. – 2007. – **253**. – P. 3987 – 3990.
20. *Arshad M., Azam A., Ahmed A.S., Mollah S., Naqvi A.H.* // J. Alloys and Compounds. – 2011. – **509**. – P. 8378 – 8381.
21. *Wang B., Callahan M.J., Xu C., Bouthillette L.O., Giles N.C., Bliss D.F.* // J. Crystal Growth. – 2007. – **304**. – P. 73 – 79.
22. *Fragalà M.E., Aleeva Y., Malandrino G.* // Thin Solid Films. – 2011. – **519**. – P. 7694 – 7701.
23. *Zhu B.L., Zhao X.Z., Su F.H., Li G.H., Wu X.G., Wu J., Wu R.* // Vacuum. – 2010. – **84**. – P. 1280 – 1286.
24. *Liang H.W., Lu Y.M., Shen D.Z., Li B.H., Zhang Z.Z., Shan C.X., Zhang J.Y., Fan X.W., Du G.T.* // Solid State Commun. – 2006. – **137**. – P. 182 – 186.
25. *Cullity B.D., Stock S.R.* Elements of X-Ray Diffraction, 3rd Ed., Prentice-Hall Inc, 2001. – P. 167 – 171.
26. *Li W.J., Shi E.W., Zhong W.Z., Yin Z.W.* // Growth, J. Crystal Growth. – 1999. – **203**. – P. 186 – 196.